Supplementary Information

Tuning the Coordination Number of Fe Single Atoms for the Efficient Reduction of CO_2

Huihuang Chen, Xu Guo, Xiangdong Kong, Yulin Xing, Yan Liu, Bolong Yu, Qun-Xiang Li, Zhigang Geng, Rui Si,* and Jie Zeng**

H. Chen,[†] X. Guo,[†] X. Kong, Y. Xing, Y. Liu, B.Yu, Q.-X. Li, Z. Geng, Prof. J. Zeng
Hefei National Laboratory for Physical Sciences at the Microscale, CAS Key Laboratory of Strongly-Coupled Quantum Matter Physics, Key Laboratory of Surface and Interface Chemistry and Energy Catalysis of Anhui Higher Education Institutes, Department of Chemical Physics, University of Science and Technology of China, Hefei, Anhui 230026, P. R. China.
E-mail: gengzg@ustc.edu.cn; zengj@ustc.edu.cn

Prof. R. Si
Shanghai Synchrotron Radiation Facility, Shanghai Institute of Applied Physics, Chinese Academy of Sciences, Shanghai 201204, P. R. China.
E-mail: sirui@sinap.ac.cn

[†]These authors contributed equally to this work.

This PDF file includes:

1. Materials characterizations

X-ray diffraction (XRD) patterns of samples were recorded on a Philips X'Pert Pro Super diffractometer with Cu-Kα radiation (λ=1.54178 Å). Scanning electron microscopy (SEM) images were obtained on JSM-6700F operated at 5kV. Transmission electron microscopy (TEM) images were taken using a transmission electron microscope (Hitachi H-7650, Japan, 100 kV). HAADF-STEM images were carried out on a field-emission transmission electron microscope (JEOL ARM-200F, Japan, 200 kV). Iron content in the samples was determined by the inductively coupled plasma-atomic emission spectroscopy (ICP-AES, Atom scan Advantage, Thermo Jarrell Ash, USA). X-ray photoelectron spectroscopy (XPS)measurements were recorded on a spectrometer (Thermo ESCALAB250Xi) with an exciting source of monochromatized Al Ka (hv = 1486.6 eV). Raman spectra were collected at the excitation wavelength of 532 nm on a JYLABRAM-HR spectrometer equipped with an integral microscope. X-ray absorption fine structure (XAFS) spectra of Fe K-edge were recorded at BL14W1 beamline of Shanghai Synchrotron Radiation Facility (SSRF) in China. CO_2temperature-programmed desorption (CO_2-TPD) profiles were conducted on a MicromeriticsAutochemII 2920 chemisorption analyzer connected with a HIDEN QIC-20 mass spectrometer.

2. Calculations of turnover frequency (TOF)

The following equation was used to calculate the TOF for CO formation:

$$TOF = \frac{I_{CO} \cdot t/nF}{m_{cat.} \times \omega/M_{Fe}}$$

where I_{CO} is the partial current density for CO; n is the number of transferred electrons to yield CO (n=2); F is the Faradaic constant (96485 C mol^{-1}); $m_{cat.}$ is the catalyst mass deposited on carbon paper; ω is the mass percent of iron in the catalyst based on ICP-AES results; M is the atomic mass of iron.

3. Computational method

All first-principle calculations in this work were carried out using the Vienna *abinitio* Simulation Package (VASP) based on the spin-polarized density functional theory.[1,2] The electron-ion interactions were described by projector augmented wave potentials.[3] The generalized gradient approximation of the Perdew-Burke-Ernzerhof (PBE) form was adopted to describe the exchange-correlation functional.[4] The electron wave functions were expanded using a plane-wave basis set with an energy cut off of 400 eV.[3] In the geometric optimization, atomic positions were fully relaxed until the associated forces are less than 0.02 eV/Å. 3 × 3 × 1 Monkhorst-Pack sampled k-points were used in all of slabs system. A vacuum region greater than 15 Å was applied to avoid interactions between the neighboring slabs caused by the periodic boundary conditions.

The considered reaction steps for the electrochemical reduction of CO_2 into CO are as follows:

(1) $CO_2 + * + H^+ + e^- \rightarrow *COOH$ (Activation process)

(2) $*COOH + H^+ + e^- \rightarrow *CO + H_2O$ (Surface reaction)

(3) $*CO \rightarrow CO(g) + *$ (Desorption process)

The Gibbs free energy for each step involved during CO_2 reduction and HER at 0 V *vs.* RHE on Fe-N_5 and Fe-$N_6$was calculated as follows:

$G = E_{DFT} + ZPVE - TS_{vib}$

where E_{DFT} is the DFT-optimized total energy; $ZPVE$ is the zero-point vibrational energy; TS_{vib} (T=298.15K) represents the vibrational entropy corrections, which were calculated through the harmonic-oscillator approximation.[5] The computational results are summarized in Table S3.

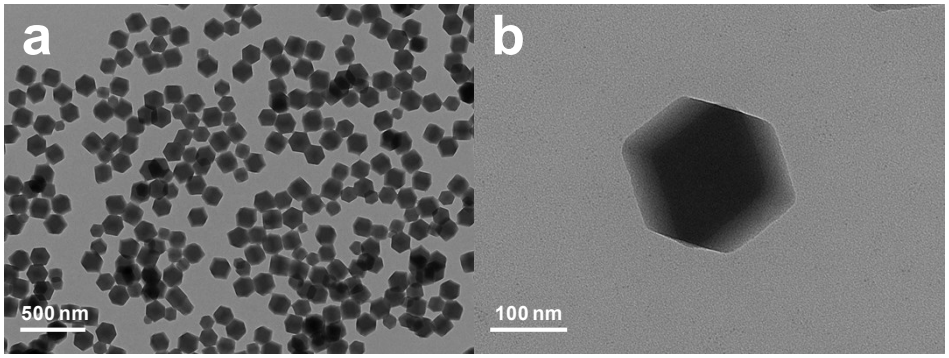

Figure S1. (**a**) TEM and (**b**) magnified TEM images of Fe-containing derivative of ZIF-8.

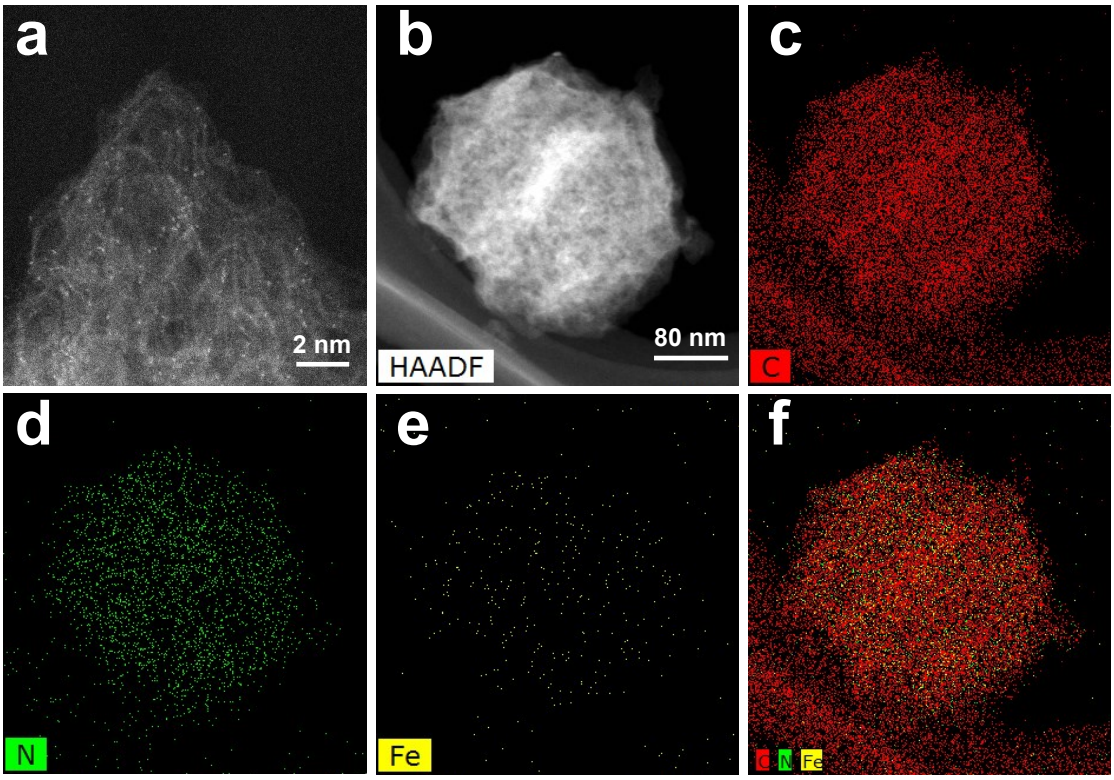

Figure S2. (**a**) Magnified HAADF-STEM image, (**b**) HAADF-STEM image, and (**c-f**) EDS mapping of Fe-N_6.

Table S1. Fitting of N 1*s* XPS spectra of Fe-N_5 and Fe-N_6.

Sample	B.E. (Ev)	Fraction (%)	Assignment
Fe-N_5	398.6	42.18	pyridinic N
	399.7	8.44	Fe-N
	400.9	35.84	pyrrolic N
	402.3	13.54	graphitic N
Fe-N_6	398.6	48.71	pyridinic N
	399.7	15.16	Fe-N
	400.9	27.05	pyrrolic N
	402.3	9.08	graphitic N

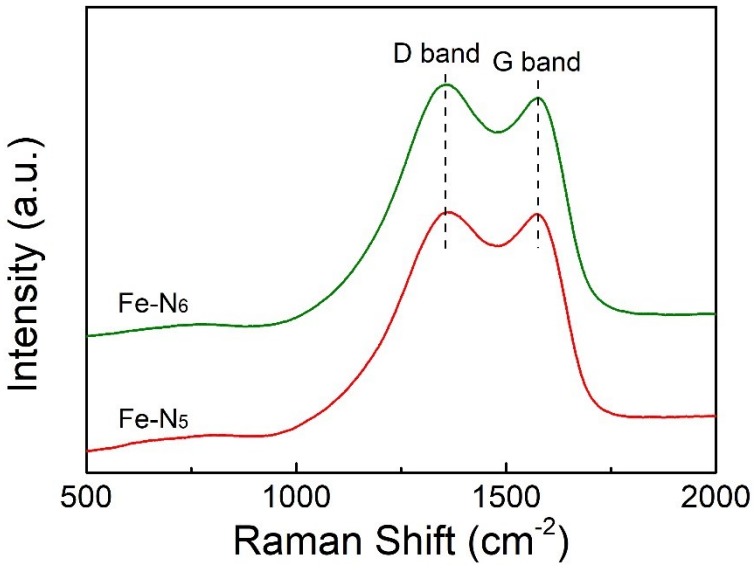

Figure S3. Raman spectra of Fe-N_5 and Fe-N_6. The intensity ratios of D band to G band (I_D/I_G) for Fe-N_5 and Fe-N_6 is 0.99 and 1.02, respectively.

Table S2. Fe K-edge EXAFS fitting results (*R*: distance; *CN*: coordination number; σ^2: Debye-Waller factor; ΔE_0: inner potential correction) for Fe-N_5 and Fe-N_6.

Sample	Fe-N		σ^2 (Å)	ΔE_0 (eV)
	R(Å)	*CN*		
Fe-N_5	2.00 ± 0.01	5.4± 0.3	0.005	10.8 ± 0.8
Fe-N_6	2.00 ± 0.01	6.0± 0.3		

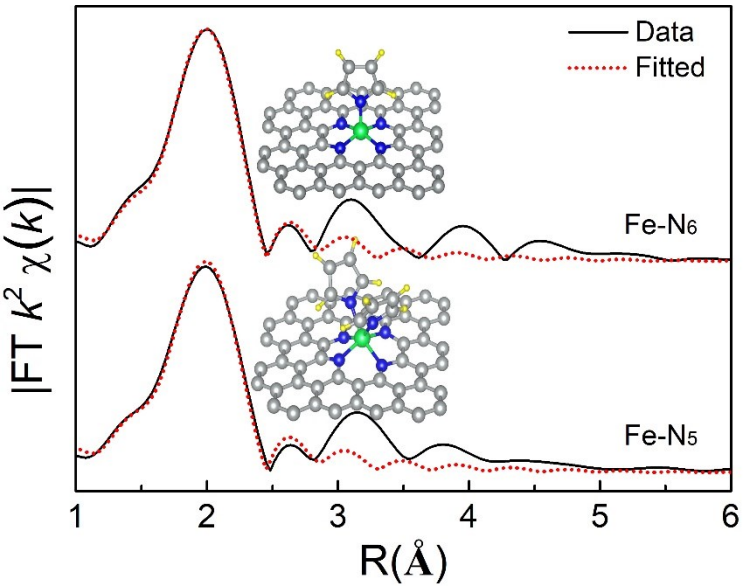

Figure S4. FT-EXAFS fitting curves for Fe-N_5 and Fe-N_6. The fitting curves match well with the experimental data. The gray, green, blue, and yellow spheres represent C, Fe, N, and H atoms, respectively.

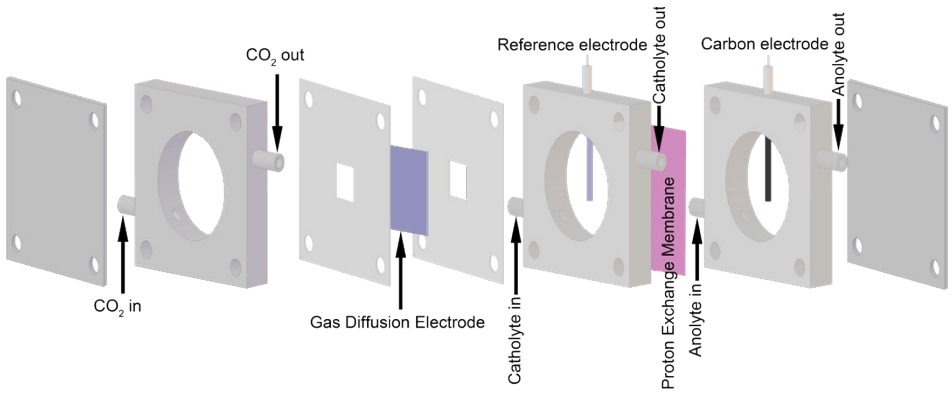

Figure S5. Scheme of the custom-designed flow cell.

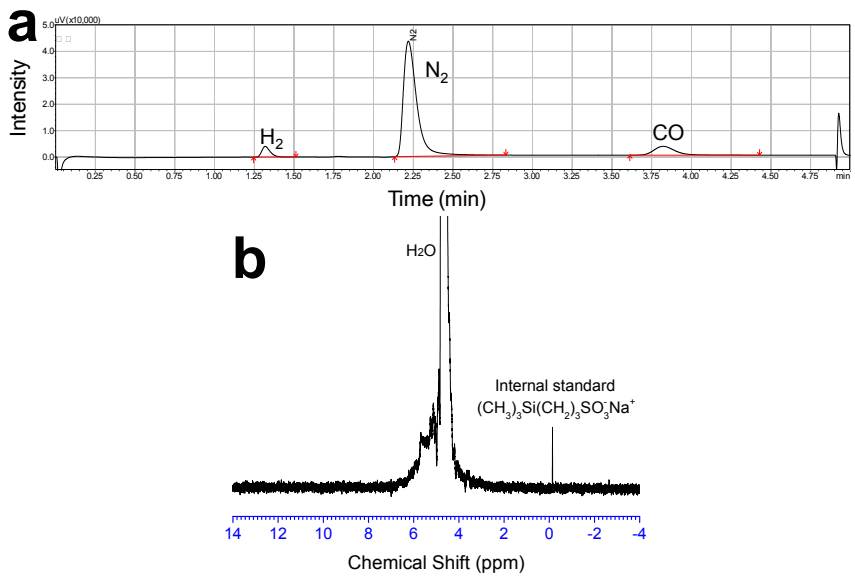

Figure S6. (**a**) On-line gas chromatography and (**b**) ^{1}H NMR spectroscopy of the electrolyte for Fe-N_5 after CO_2 electroreduction at -0.45 V *vs.* RHE.

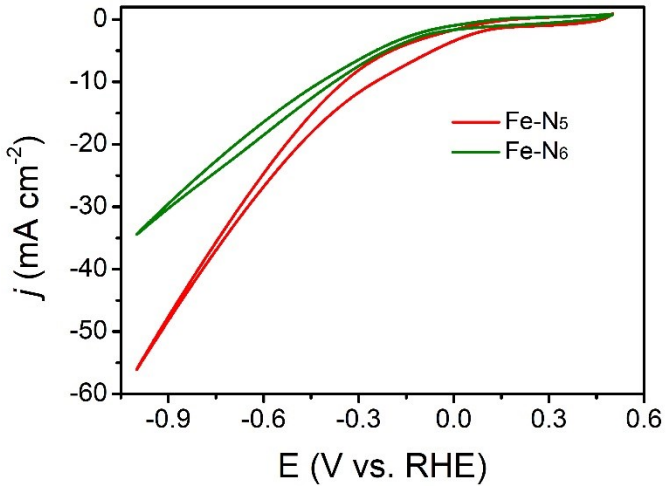

Figure S7. Cyclic voltammograms (CVs) of Fe-N_5 and Fe-N_6 recorded under CO_2 (gas flow rate=10 sccm; sweep rate=10 mV s^{-1}) in 1.0 M KOH aqueous electrolyte.

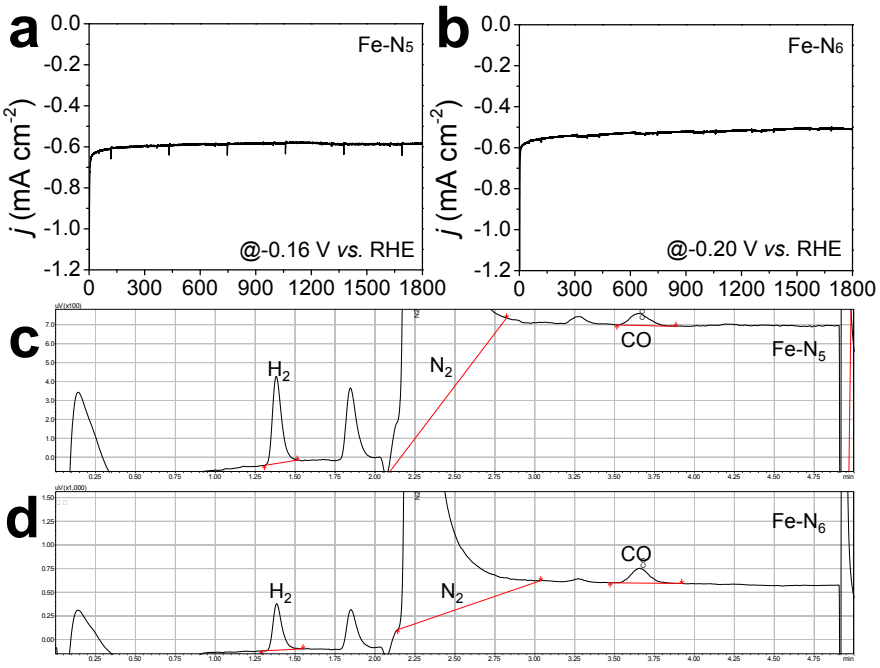

Figure S8. Chronoamperometry curves of (**a**) Fe-N_5 and (**b**) Fe-N_6 in 1.0 M KOH electrolyte. The corresponding GC curves of (**c**) Fe-N_5 and (**d**) Fe-N_6 after the electrolysis.

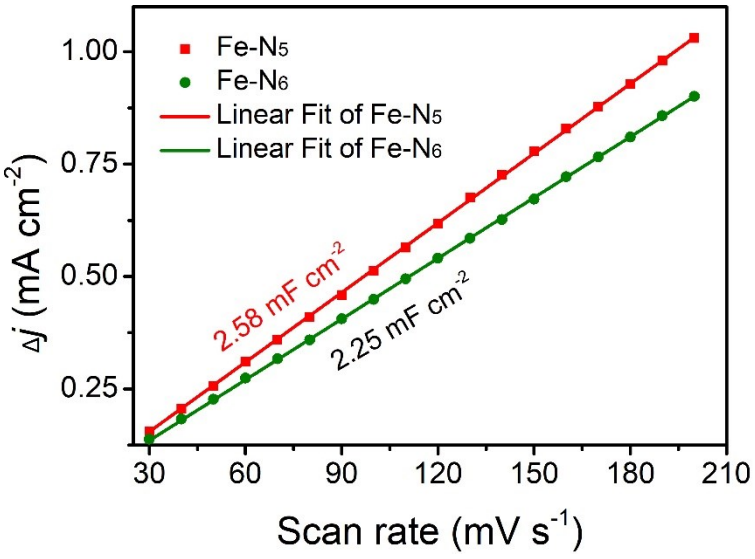

Figure S9. Linear fitting of double layer capacitive currents (Δj (j_a-j_c)) plotted against scan rates performed in CO_2-saturated 1.0 M KOH solution.

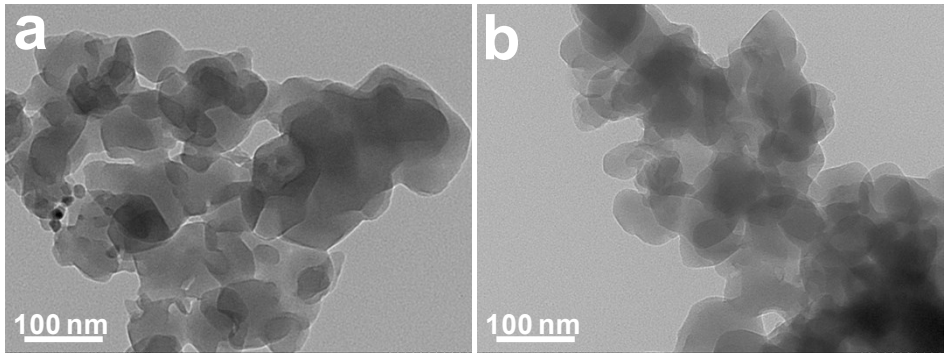

Figure S10. TEM images of (**a**) ZIF-8-800 and (**b**) ZIF-8-900.

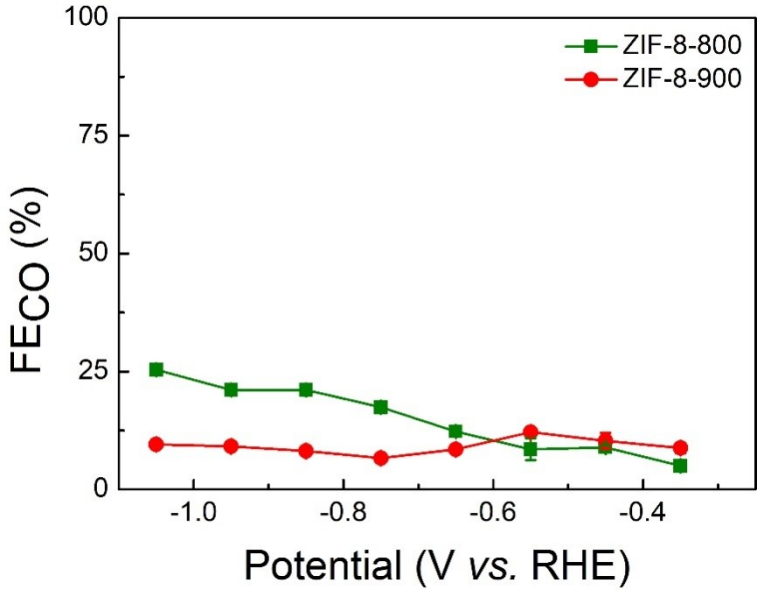

Figure S11. FE_{CO} at different applied potentials for ZIF-8-800 and ZIF-8-900.

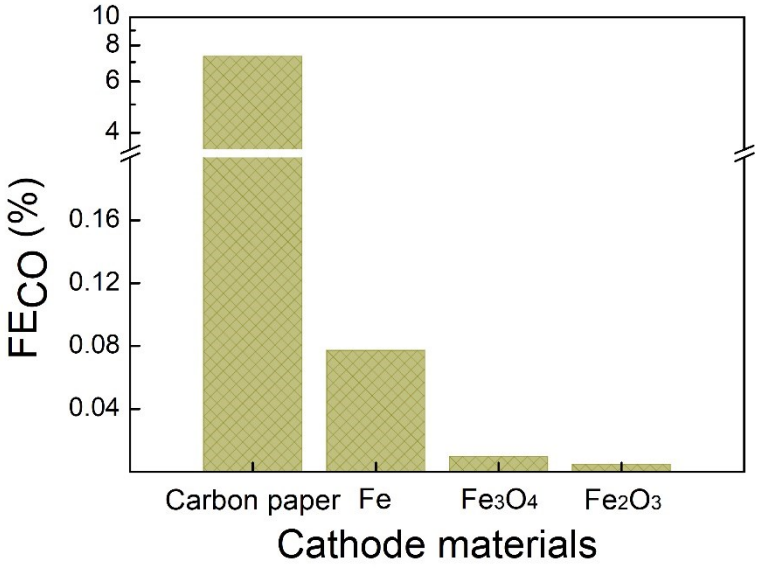

Figure S12. FE_{CO} on carbon paper, Fe, Fe_3O_4, and Fe_2O_3 at -0.55 V *vs*. RHE. The extremely low FE_{CO} confirmed the structure-sensitivity of Fe species.

Table S3. Electrocatalytic performance of Fe-N_5 and some previously reported catalysts for CO_2 electroreduction.

Catalyst	Electrolyte	Maximum FE_{CO}	Overpotential	Reference
Fe-N_5	0.5 M $KHCO_3$	94%	0.38 V	This work
H-M-G	0.1 M $KHCO_3$	96.6%	0.35 V	6
Fe-N-C	0.1 M $NaHCO_3$	91%	0.49 V	7
Fe-N-C	0.1 M $KHCO_3$	80%	0.49 V	8
Fe/NG-750	0.1 M $KHCO_3$	80%	0.46 V	9
Ni-N-G	0.1 M $KHCO_3$	90%	0.59 V	10
A-Ni-NSG	0.5 M $NaCO_3$	97%	0.61 V	11
Ni SAs/N-C	0.5 M $KHCO_3$	71.9%	0.79 V	12
Ni-NG	0.5 M $KHCO_3$	95%	0.55 V	13
Co-N_2	0.5 M $NaHCO_3$	94%	0.52 V	14
Co-N_5/HNPCSs	0.2 M $NaHCO_3$	99.4%	0.68 V	15
NiSA-N-CNTs	0.5 M $KHCO_3$	89%	0.44 V	16
CoNi-NC	0.5 M $KHCO_3$	50%	0.39 V	17
Ni-N_3-V SAC	0.5 M $KHCO_3$	94%	0.69 V	18

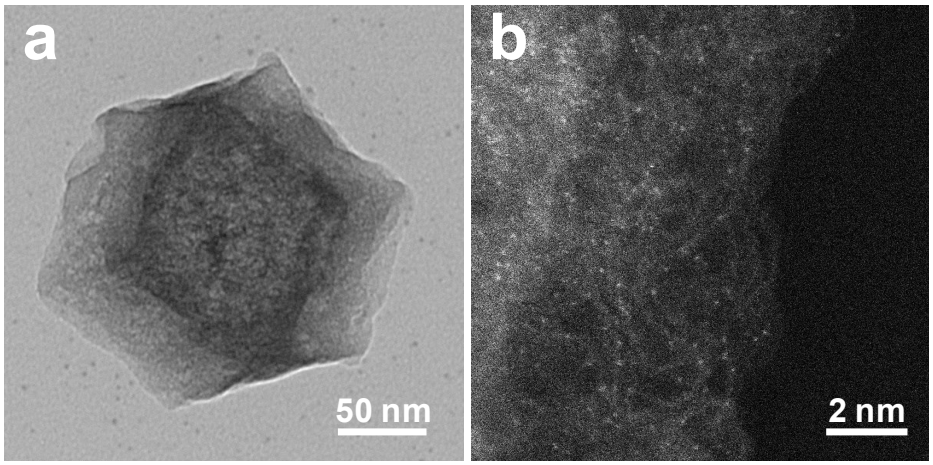

Figure S13. (**a**) TEM and (**b**) HAADF-STEM images of Fe-N_5 after the long-time stability test.

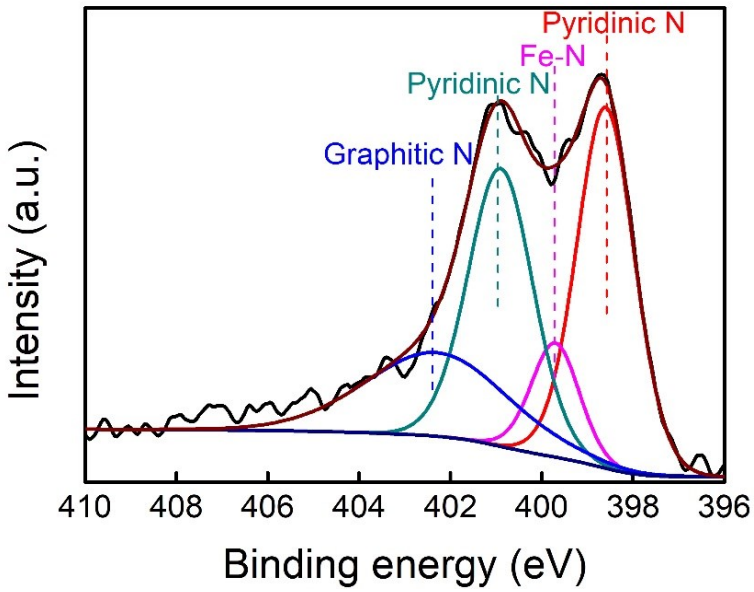

Figure S14. N 1*s* XPS spectra of spent Fe-N_5 after 24-h continuous electrolysis.

Table S4. Fitting of N 1*s* XPS spectra of spent Fe-N_5 after 24-h continuous electrolysis.

Sample	B.E. (Ev)	Fraction (%)	Assignment
Spent Fe-N_5	398.6	36.93	pyridinic N
	399.7	9.77	Fe-N
	400.9	32.04	pyrrolic N
	402.3	21.25	graphitic N

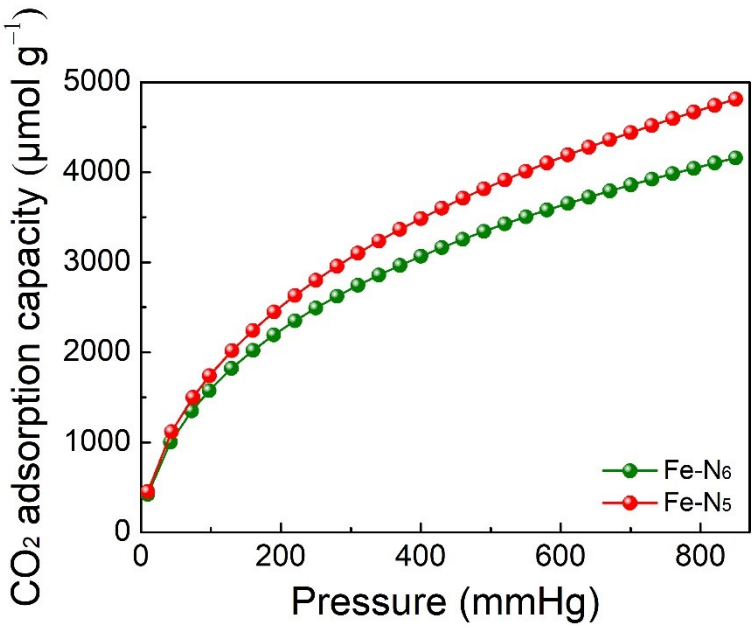

Figure S15. CO_2 adsorption isotherms of Fe-N_5 and Fe-N_6 collected at 298 K.

Table S5. The thermodynamic contributions to the free energy for the molecules and adsorbates from the DFT calculations (T=298.15 K).

Species	E_{DFT} (eV)	*ZPVE* (eV)	$-TS_{vib}$ (eV)
H_2(g)	-6.76	0.27	-0.4
CO_2(g)	-22.99	0.31	-0.66
CO(g)	-14.80	0.14	-0.61
H_2O(g=l)	-14.22	0.57	-0.22
Fe-N_5	-597.12	0	0
Fe-N_5-∗COOH	-622.71	-0.22	0.62
Fe-N_5-∗CO	-612.64	-0.14	0.23
Fe-N_6	-653.84	0	0
Fe-N_6-∗COOH	-678.45	-0.20	0.63
Fe-N_6-∗CO	-667.17	-0.14	0.21

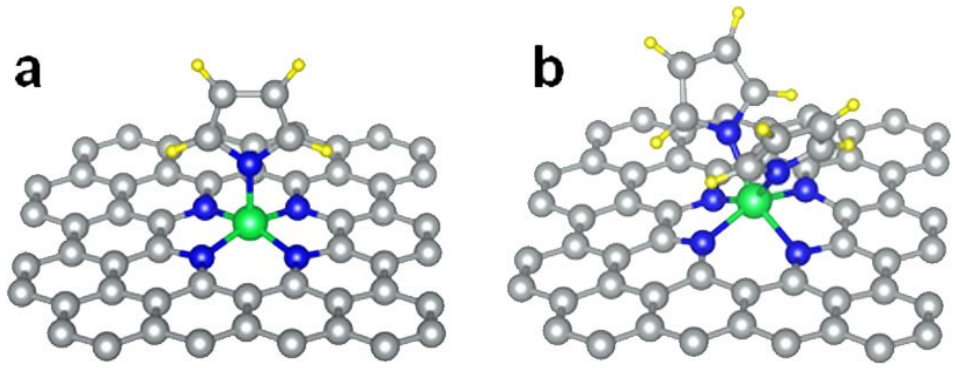

Figure S16. The lateral view of (**a**) Fe-N_5 and (**b**) Fe-N_6 established based on XPS and EXAFS fitting results. The gray, green, blue, and yellow spheres represent C, Fe, N, and H atoms, respectively.

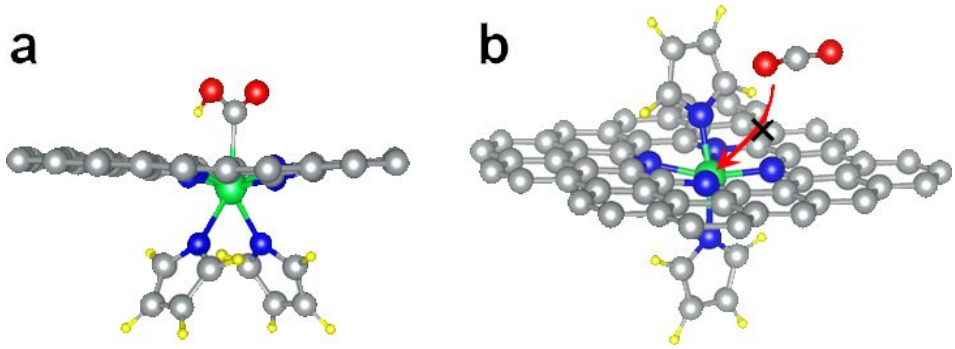

Figure S17. Two kinds of structural models of Fe-N_6. Theoretical calculations showed that Fe-N_6 with two pyrrole rings on the same side can activate CO_2 while Fe-N_6 with one pyrrole ring on each side cannot.

References:

[1] G. Kresse, J. Furthmüller, *Phys. Rev. B*., 1994, **54**, 11169-11186.

[2] G. Kresse, J. Furthmüller, *Comp. Mater. Sci*., 1996, **6**, 15-50.

[3] P. E. Blöchl, *Phys. Rev. B*., 1994, **50**, 17953-17979.

[4] J. P. Perdew, K. Burke, M. Ernzerhof, *Phys. Rev. Lett*., 1996, **77**, 3865-3868.

[5] J. K. Nørskov, T. Bligaard, A. Logadottir, J. Kitchin, J. Chen, S. Pandelov, U. Stimming, *J. Electrochem. Soc.*, 2005, **152**, J23-J26.

[6] H. Zhang, J. Li, S. Xi, Y. Du, X. Hai, J. Wang, H. Xu, G. Wu, J. Zhang, J. Lu, J. Wang, *Angew. Chem. Int. Ed.*, 2019, **58**, 14871-14876.

[7] T. N. Huan, N. Ranjbar, G. Rousse, M. Sougrati, A. Zitolo, V. Mougel, F. Jaouen, M. Fontecave, *ACS Catal.*, 2017, **7**, 1520-1525.

[8] A. S. Varela, N. Ranjbar Sahraie, J. Steinberg, W. Ju, H.-S. Oh, P. Strasser, *Angew. Chem. Int. Ed.*, 2015, **54**, 10758-10762.

[9] C. Zhang, S. Yang, J. Wu, M. Liu, S. Yazdi, M. Ren, J. Sha, J. Zhong, K. Nie, A. S. Jalilov, Z. Li, H. Li, B. I. Yakobson, Q. Wu, E. Ringe, H. Xu, P. M. Ajayan and J.M. Tour, *Adv. Energy Mater.*, 2018, **8**, 1703487.

[10] P. Su, K. Iwase, S. Nakanishi, K. Hashimoto, K. Kamiya, *Small*, 2016, **12**, 6083-6089.

[11] H. B. Yang, S.-F. Hung, S. Liu, K. Yuan, S. Miao, L. Zhang, X. Huang, H.-Y. Wang, W. Cai, R. Chen, J. Gao, X. Yang, W. Chen, Y. Huang, H. M. Chen, C. M. Li, T. Zhang and B. Liu, *Nat. Energy*, 2018, **3**, 140-147.

[12] C. Zhao, X. Dai, T. Yao, W. Chen, X. Wang, J. Wang, J. Yang, S. Wei, Y. Wu, Y. Li, *J. Am. Chem. Soc.*, 2017, **139**, 8078-8081.

[13] K. Jiang, S. Siahrostami, T. Zheng, Y. Hu, S. Hwang, E. Stavitski, Y. Peng, J. Dynes, M. Gangisetty, D. Su, K. Attenkofer, H. Wang, *Energy Environ. Sci.*, 2018, **11**, 893-903.

[14] X. Wang, Z. Chen, X. Zhao, T. Yao, W. Chen, R. You, C. Zhao, G. Wu, J. Wang, W. Huang, J. Yang, X. Hong, S. Wei, Y. Wu, Y. Li, *Angew. Chem. Int. Ed.,*, 2018, **57**, 1944-1948.

[15] Y. Pan, R. Lin, Y. Chen, S. Liu, W. Zhu, X. Cao, W. Chen, K. Wu, W.-C. Cheong, Y. Wang, L. Zheng, J. Luo, Y. Lin, Y. Liu, C. Liu, J. Li, Q. Lu, X. Chen, D. Wang, Q. Peng, C. Chen, Y. Li, *J. Am. Chem. Soc.*, 2018, **140**, 4218-4221.

[16] Y. Cheng, S. Zhao, B. Johannessen, J. P. Veder, M. Saunders, M. R. Rowles, M. Cheng, C. Liu, M. F. Chisholm, R. De Marco, *Adv. Mater.*, 2018, **30**, 1706287.

[17] Q. He, D. Liu, J. H. Lee, Y. Liu, Z. Xie, S. Hwang, S. Kattel, L. Song, J. G. Chen, *Angew. Chem.*, 2020, **132**, 3057-3061.

[18] X. Rong, H.-J. Wang, X.-L. Lu, R. Si, T.-B. Lu, *Angew. Chem. Int. Ed.*, 2020, **59**, 1961-1965.